



Enhancing sustainability in polymer 3D printing via fusion filament fabrication through integration of by-products in powder form: mechanical and thermal characterization

Laura Castanon-Jano^{1,2} · Paula Palomera-Obregon^{1,2} · Mariano Lázaro^{1,3} · Elena Blanco-Fernandez² · Sergio Blasón⁴

Received: 22 January 2024 / Accepted: 12 April 2024 / Published online: 28 May 2024

© The Author(s) 2024

Abstract

FFF (fused filament fabrication) is a type of 3D printing that utilizes filament for part creation. This study proposes using by-products or waste to replace part of the plastic in FFF filament, reducing environmental impact. The aim is to maintain a simple manufacturing process involving extrusion on a single-screw desktop machine followed by printing. The plastic matrix comprises polylactic acid (PLA) and polyethylene glycol (PETG), with added powdered by-products: seashells, car glass and mill scale (metal). Additives will be incorporated at 10% and 20% by weight, with two grain sizes: up to 0.09 mm and up to 0.018 mm. Mechanical tests (tensile, flexural and hardness) and thermal characterization tests will be conducted. Findings suggest adding 10%w powder of any variety to PETG increases tensile strength up to 48%, with metal powder (mill scale) showing the highest enhancement, even at 20%w, resulting in a 41% increase. Conversely, adding powder to PLA worsens mechanical properties without stiffening the material; instead, the elastic modulus decreases. Metal grain size has minimal impact, with grain sizes lower than 0.09 mm optimal for PLA. Thermal conductivity in polymers blended with powder additives is lower than in virgin polymers, likely due to air void formation, supported by density and microscopic evaluations. This research underscores the potential of utilizing waste materials with a simple FFF filament production to enhance sustainability in 3D printing practices.

Keywords 3D printing · FFF · PLA · PETg · Metal powder · Glass powder · Seashells powder · Tension · Bending · Thermal properties · Sustainability · Plastic consumption

1 Introduction

Additive manufacturing (AM), particularly fused filament fabrication (FFF), has emerged as a transformative technology, offering versatile solutions across various sectors

ranging from engineering to healthcare [1, 2]. FFF operates by extruding thermoplastic filaments layer by layer, allowing for the creation of intricate three-dimensional structures with high precision and customization. This technology has revolutionized traditional manufacturing processes by enabling rapid prototyping, on-demand production and complex geometries, thus significantly reducing lead times and costs associated with conventional methods

One of the key advantages of FFF lies in its capacity to utilize plastic materials in diverse ways for myriad applications, thereby potentially mitigating the environmental impact associated with plastic consumption [3]. However, the widespread adoption of FFF has raised concerns about the substantial amount of plastic waste generated, prompting research efforts to explore sustainable alternatives. This paper aims to address this challenge by proposing a novel approach: incorporating by-product powders derived from industrial processes into polymer 3D printing filaments.

✉ Laura Castanon-Jano
laura.castanon@unican.es

¹ Area of Manufacturing Processes, School of Industrial Engineering and Telecommunications, University of Cantabria, 39005 Santander, Spain

² GITECO Research Group, School of Civil Engineering, University of Cantabria, 39005 Santander, Spain

³ GIDAI, Universidad de Cantabria, Avda. Los Castros, s/n, 39005 Santander, Spain

⁴ Department of Component Safety, Bundesanstalt für Materialforschung und -prüfung (BAM), Unter den Eichen 87, 12205 Berlin, Germany

The concept of utilizing by-products as additives introduces a paradigm shift in material development for FFF. Unlike conventional additives specifically manufactured for this purpose, the additives in this study are repurposed from other industrial processes, tapping into underutilized resources and contributing to the circular economy. This innovative approach not only offers environmental benefits by reducing waste but also adds value to materials that would otherwise be discarded.

While previous studies have explored the incorporation of various additives into polymer filaments for FFF, they often relied on additives specifically designed for this application: extant literature predominantly discusses the integration of metallic additives [4–7], organic plant-derived materials [8–10] or marine shells [11] or utilized recycled plastics in different origins such as bottle caps [12] or milk pouches [13] or from supports or failed prints from the same 3D printing process [14, 15], to assess their suitability for extrusion into filament and subsequent printing, while evaluating their mechanical properties. Additionally, the utilization of waste powders has been limited, with only sporadic instances such as the incorporation of coffee grounds [16]. In contrast, this paper introduces a pioneering method that focuses on reducing plastic consumption by leveraging by-products from other industrial processes, such as steel mill scale, seashells and crushed automotive glass.

Another significant contribution of this paper lies in its simplified manufacturing process. While existing literature often complicates filament production by pre-processing of the plastic-powder mixture [17, 18], postprocessing of the 3D printed part [19–21], dual extrusion processes or double screw extruders [5, 8, 9, 22–25], physico-chemical treatments [8–11, 22] or even printing plastic with added continuous filament or supplementing the printed piece with additional layers of different materials to form sandwich panels [26–28], this study adopts a straightforward approach using a single-screw extruder. Despite the clear improvement observed in the performance of the resulting parts previously mentioned, the level of manufacturing complexity falls outside the scope of this study. Manufacturing processes can become as complex as necessary depending on the intended applications. By streamlining the manufacturing process, this paper aims to develop a versatile material incorporating various industrial by-products while ensuring ease of production and scalability.

Taking the previous key points into consideration, this study comprehensively investigates the mechanical and thermal properties of the developed filaments. By evaluating these properties, the study aims to ascertain whether the incorporation of industrial by-products enhances or maintains the performance of the filaments, thereby ensuring their suitability for a wide range of applications. Ultimately,

the utilization of these filaments not only offers environmental benefits through waste reduction but also presents opportunities for enhanced sustainability in additive manufacturing practices.

In summary, this paper presents a pioneering approach to polymer 3D printing filament development, leveraging industrial by-products to reduce plastic consumption and promote environmental sustainability. By adopting a simplified manufacturing process and conducting thorough property analyses, this study aims to contribute to the advancement of sustainable materials for additive manufacturing applications.

2 Materials and methods

2.1 Materials

In FFF printing technology, polymers such as PLA [3, 29], ABS [30, 31], PETg [32, 33], PET [34, 35] or TPU [30, 36] are used. The choice of polymeric matrices in this paper is made considering three main aspects: printability, biodegradability (environmentally friendly) and health impact. Elastomers are out of the scope of this work, discarding the use of TPU. Also, PET is discarded due to its brittleness and higher shrinkage risk [37], as well as ABS because it contains carcinogenic substances [38]. Hence, PLA and PETg were selected to be used as plastic matrices. Both polymers were supplied in pellets shape (Fig. 1) by the company EOLAS Prints (Cantabria, Spain).

PLA is a biopolymer made from renewable resources such as corn starch, sugarcane and cassava. It is widely used in applications such as food packaging, disposable cutlery and medical implants [39]. PETG, on the other hand, is a thermoplastic polymer that is known for its durability, toughness and chemical resistance. It is commonly used in applications that require high strength and impact resistance, such as medical equipment, electronics and automotive parts [40, 41].

Despite the biopolymeric nature of PLA, certain authors have evidenced that its environmental impact equals or surpasses that of PETg [42, 43]. Given this context, it is recognized that reducing plastic consumption in both scenarios is equally desirable, as supported by findings demonstrating its impact mitigation [3]. In line with this perspective, this study aims to address plastic reduction by incorporating three types of additives, derived as by-products from diverse industrial processes (see Fig. 1).

- *Glass powder*, which comes from the shredding of car windows, was supplied by the waste management company FCC Ámbito S.A. (Cantabria, Spain) and was used

Fig. 1 Raw materials: PLA and PETg pellets and metal, seashell and glass powder



as an additive. After crushing, the coarser fraction can be re-melted and re-used to produce more glass. However, this is not feasible for the finer fraction that is usually recycled in other applications (i.e. ceramic industry, construction materials, among others). After carrying out 3D printing work on concrete incorporating this material [44, 45], it was decided to also incorporate it into the FFF 3D printing process for plastic, in order to analyse its behaviour.

- *Seashells powder*: in this instance, the source of the additives was the company Abonomar (Galicia, Spain), which specializes in producing chicken fodder. The additives used in the study consisted of natural products, including calcium carbonate, tiger mussel shells, fertilizers and oyster grit. These materials are particularly appealing for incorporation due to their biodegradable properties.
- *Metal powder*, coming from Celsa Group (Barcelona, Spain). The material utilized in this study is derived from the steel rolling process and is commonly referred to as scale. This substance is formed

when iron oxide reacts with extremely hot metal during casting, annealing and hot rolling processes, and can vary in size from a few microns to several centimetres. Failure to remove this substance prior to subsequent rolling operations can lead to significant damage to the steel finished surface. However, in this study, the scale has been repurposed by incorporating it into the polymeric matrix, providing it with a second life and a new use.

The materials were mixed in varying proportions and granulometries, as shown in Table 1. A total of 20 cases were manufactured, 10 for each polymer matrix.

The choice of study cases is made by systematically combining all parameters to explore every possible combination. While the design of experiments (DOE) technique has been utilized in many other studies [3, 46, 47], it is primarily aimed at optimizing printing parameters based on specific material characteristics. However, in this research, the emphasis is placed on assessing the real response of all combinations.

Table 1 Cases object of study

Polymer matrix	Type of additive	Additive in weight (%)	Grain size (mm)
PLA cases (1–10) or PETg (cases 11–20)	Virgin	-	-
	Seashells powder	10	0.18
		20	0.09
		20	0.18
	Glass	10	0.18
		20	0.09
		20	0.18
	Metal	10	0.18
		20	0.09
		20	0.18

2.2 Manufacturing of filament and samples

Before the extrusion process, the PLA was dried at 60 °C and PETg at 70 °C for 24 h, to remove as much moisture as possible and reduce the presence of pores in the filament.

The filament was produced using pure PLA or PETg with the correspondent additive at the specified percentage for each case, utilizing the 3devo Composer 450 desktop extruder. The device contains a single extrusion screw that features a grooved shape at the end, which is specially designed to manufacture plastic mixtures with other powder components. A small hopper receives the material, which then passes through a grid into the extrusion screw. The extrusion screw operates with four different temperatures on four different points along its longitudinal direction.

In the case of PLA polymer matrix, the screw temperatures used in this study for the plain material, ordered from the beginning to the end of the extrusion screw, are 170, 185, 190 and 170 °C. Subsequently, the extruded material exits through the nozzle, where it is cooled by two fans and the diameter is monitored by a sensor integrated into the machine. Furthermore, the extruder itself has a winding system for the extruded product that is adapted to the material output speed. In order to produce a uniformly consistent filament with an even diameter, which meets the essential criteria for its utilization in 3D printing, the screw temperatures were adjusted for each additive (Table 2). The primary aim was to achieve a temperature at the initial stage that would facilitate the polymer proper melting and homogeneous mixing with the associated powder. The temperature must not be excessively high as to result in overly fluid extrusion through the nozzle. The fan speed was also modified in the case of the glass 20% and in the case of the shells 20% wt. In both cases, fan speed was set to 50%. Normally, this value is set at 80% for PLA and 90% for PETg matrix.

Similarly, PETg was utilized in this study. However, due to the nature of this polymeric matrix, higher temperatures are required in the extrusion process than in the case of PLA. The extruder temperatures used for PETg were 220 °C, 230 °C, 235 °C and 220 °C, which were found to consistently produce homogeneous mixtures without the need for modification in each case.

The machine used to fabricate the specimens was the Artillery Sidewinder X1 3D printer. The pre-processing

Table 2 Screw temperatures for the extrusion process

PLA	T1 (°C)	T2 (°C)	T3 (°C)	T4 (°C)
Metal 20%	175	193	187	178
Metal 10%	175	185	190	175
Glass 20%	175	185	187	172
Seashells 20%	179	187	193	182

software used was Ultimaker Cura, which imported the specimens in STL format, positioned them on the printing bed and defined the printing parameters.

Table 3 displays the unchanging parameters that have been maintained consistently throughout all of the cases examined. The bed temperature remained at 60 °C for PLA and 80 °C for PETg, while the nozzle temperatures remained fixed at 210 °C and 235 °C, respectively.

Manufactured samples for tensile, bending and hardness tests with PLA can be seen on Fig. 2.

2.3 Experimental tests

The UNE-EN ISO 527-2:2019 [48] standard was used for conducting *tension tests*. The type 1B specimen geometry with a halter shape was selected. For the *bending tests*, the UNE-EN-ISO 178:2019 [49] standard was employed, which requires prismatic geometry for the specimens.

The tests were carried out using the Zwick Roell Z100 universal testing machine. The tension tests were performed by securely clamping the ends of the specimens between two flat grips, maintaining a specimen base test length of 115 mm. The base length between optical gauges to measure deformations was set to 50 mm. The bending tests were conducted on an 80 mm length × 10 mm width specimen, with a 64 mm separation between supports and a punctual load applied at the centre of the specimen.

A *digital microscope* VHX-7000 was used to evaluate the geometry, fracture zone and powder distribution in the polymeric matrix of the tension samples.

The *hardness* behaviour of the material is also evaluated. For this purpose, the standard UNE-ISO 7619-1 is used. For each specimen, six measurements are taken on the side next to the printing bed and other six on the opposite side. A shore D durometer was used for this purpose.

Thermal diffusivity and specific heat were determined by means of a laser flash analysis (LFA) [50], following the standard ISO 22007-4:2017 using NETZSCH LFA 447

Table 3 Parameters kept constant in all the printed parts

Parameters	Magnitude
Nozzle size	1.2 mm
Infill density	100%
Layer height	0.4 mm
Number of contour lines	1
Infill line directions	[45°, -45°]
Printing speed	45 mm/s
Contour speed	30 mm/s
Retraction distance	0.2 mm
Retraction speed	25 mm/s
Build orientation	Horizontal

Fig. 2 Tensile, bending and hardness samples made with PLA and PLA+additives



NanoFlash. The test is based on the emission of a heat pulse given by a Xenon flash lamp towards a disk shape sample. The measurement of the temperature increase on the rear of the sample is carried out with a liquid-nitrogen cooled InSb infrared detector. The dimensions of the disk shape samples manufactured by 3D printing are 12.7 mm diameter and approximately 1.2 mm height.

Thermal diffusivity a (in mm^2/s) is determined using Equation (1):

$$a = 0.1388 \cdot \frac{d^2}{t_{\frac{1}{2}}} \tag{1}$$

being d the thickness of the sample in mm and $t_{\frac{1}{2}}$ the time to half minimum in s. Then, thermal conductivity λ (in W/mK) can be calculated using Equation (2):

$$\lambda = a \cdot c_p \cdot \rho \tag{2}$$

being a the thermal diffusivity in mm^2/s , c_p the specific heat in J/gK and ρ the density of the sample in g/cm^3 .

The three thermal properties were determined at five different temperatures: 30, 45, 60, 75 and 90 °C. In order to guarantee the repeatability of the results, two specimens of each material were tested and three pulses were emitted at each temperature to capture the results.

Thermogravimetric analysis (TGA) and differential scanning calorimetry (DSC) were carried out simultaneously with STA 449 F3 Jupiter. A sample of approximately 6 g was deposited in a microbalance and inserted in the furnace. The temperature was increased with a heating rate of 10 K/min. The change of mass was registered every

5°C, as well as the released or absorbed energy, quantified by comparison with a reference sample. Registers were taken from ambient temperature to 800 °C.

3 Results

3.1 Mechanical tests

For each specimen, the stress-strain curve was obtained for the case of tension or force-deflection for the case of bending. Subsequently, calculations were performed using equations derived from the UNE-EN ISO 527-2:2019 [48] and UNE-EN-ISO 178:2019 [49] standards to determine the values of interest, including maximum strength (σ), elastic modulus (E) and strain at the point of maximum strength (ϵ). Table 4 presents the mean values and percentage deviations of the five replicates of each DoE case for each of the six mechanical outputs. Notably, some results were excluded from the analysis due to testing issues, such as premature breakage or breakage in the jaw area, or results that were significantly deviant from other specimens in the same case (outliers).

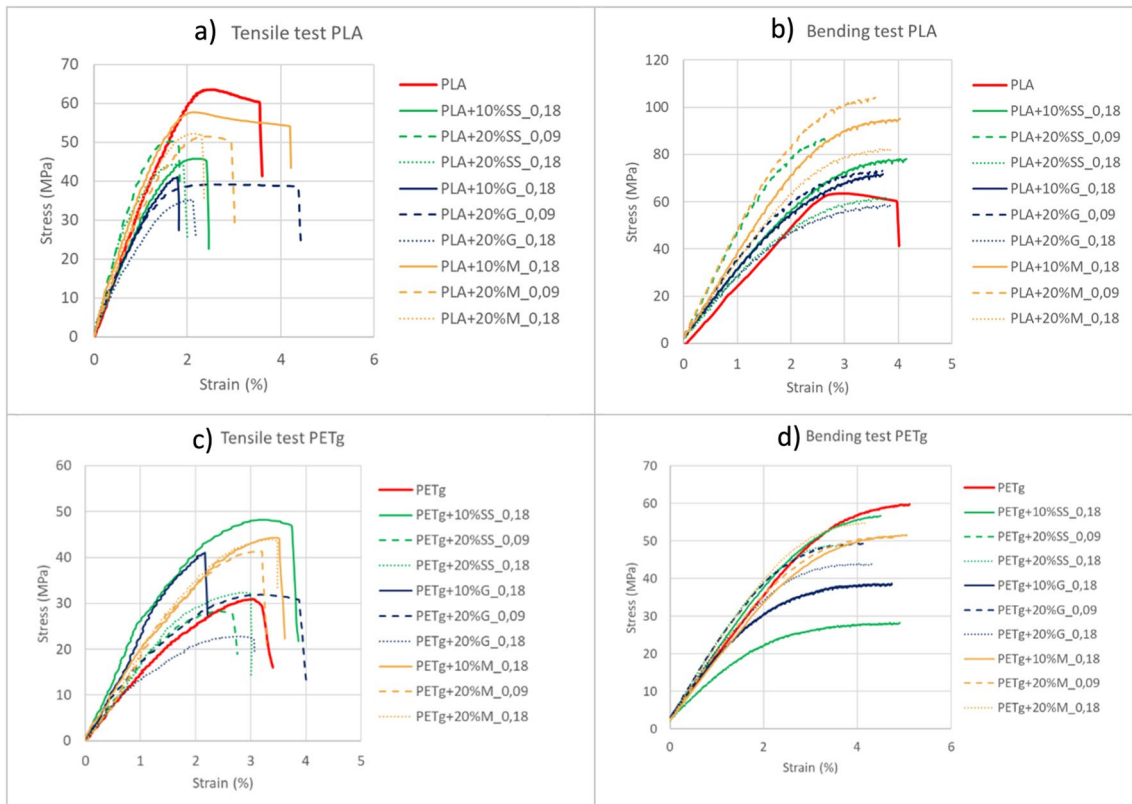
3.2 Evaluation according to quantity and type of additive

This section tries to analyse the tensile and bending mechanical properties (Fig. 3) as a function of the polymer and powder percentage used.

Table 4 Results (strength, elastic modulus and strain) of the tension and bending tests

Matrix	Type	A (%)	S_g (mm)	Tension			Bending		
				σ_t (MPa)	E_t (MPa)	ϵ_t (%)	σ_f (MPa)	E_f (MPa)	ϵ_f (%)
PLA	-	-	-	64.27±3%	3493.02±5%	2.60±17%	97.41±3%	3552.42±3%	4.13±1%
	S	10	0.18	44.21±7%	3239.29±3%	2.00±10%	75.31±4%	3235.52±8%	4.14±6%
		20	0.09	48.10±8%	4359.34±9%	1.67±7%	80.72±3%	4700.28±4%	2.74±6%
		20	0.18	41.48±14%	3677.77±9%	1.87±7%	60.13±13%	3145.22±14%	3.72±7%
	G	10	0.18	43.47±8%	2585.68±15%	2.09±27%	81.15±3%	3714.04±11%	3.79±6%
		20	0.09	38.88±3%	2483.36±4%	2.70±11%	74.13±3%	4321.13±5%	3.64±4%
		20	0.18	32.83±12%	2335.71±5%	2.20±20%	56.53±5%	3318.82±5%	3.97±5%
	M	10	0.18	56.88±3%	3151.77±2%	2.07±7%	91.52±2%	3940.65±5%	4.18±3%
		20	0.09	51.86±4%	3096.42±4%	2.26±10%	99.97±4%	4564.32±14%	3.74±4%
20		0.18	52.69±3%	3271.26±5%	2.19±11%	89.46±3%	3850.31±7%	3.87±4%	
PETg	-	-	-	30.12±8%	1447.87±9%	3.02±8%	58.00±5%	2018.07±5%	4.78±12%
	S	10	0.18	43.89±9%	2296.02±9%	2.89±15%	60.18±8%	2545.38±6%	4.62±3%
		20	0.09	25.46±16%	1471.93±9%	2.26±26%	24.57±35%	1379.59±37%	3.08±37%
		20	0.18	28.15±34%	1392.72±21%	2.76±20%	44.85±13%	2100.51±14%	3.53±6%
	G	10	0.18	34.95±3%	1906.71±4%	3.00±6%	37.69±6%	1987.68±4%	4.32±10%
		20	0.09	32.12±3%	1987.76±2%	2.97±7%	48.29±10%	2548.69±7%	3.53±9%
		20	0.18	24.23±8%	1400.71±5%	2.84±7%	43.87±4%	2309.88±4%	3.53±5%
	M	10	0.18	44.50±6%	1954.82±5%	3.36±4%	52.38±7%	2060.03±3%	3.35±3%
		20	0.09	41.33±8%	1610.96±3%	3.09±11%	50.17±2%	2136.11±4%	3.06±4%
		20	0.18	42.44±5%	1778.89±14%	3.22±5%	53.36±4%	2442.29±3%	3.53±3%

A (%), additive percentage; S_g (mm), grain sizes, S seashells powder, G glass powder, M metal powder

**Fig. 3** Representative stress-strain curves corresponding to tensile (a and c) and bending tests (b and d)

3.2.1 Tensile properties

The present section aims to assess the tensile mechanical properties of the filament combinations obtained as explained in Section 3.1. Subsequently, the variation of each parameter concerning the proportion of the corresponding additive included is illustrated in Fig. 4 for each type. It is important to note that the data points displayed in each graph refers to the mean value obtained from a set of five specimens for each scenario.

With respect to PLA (Fig. 4a), there exists an inverse correlation between the weight percentage of an additive and the corresponding tensile strength. The most substantial decline is observed upon incorporation of glass powder, as evidenced by a strength reduction of 49% in filaments loaded at 20% by weight, relative to the pure material. By contrast, the strength reduction for metal and shell powder is 18% and 35%, respectively.

The reduction witnessed in strength as the load increases is non-linear. The decrease is higher in the first addition of powder for the three cases than when it changes from 10 to 20% wt.

This behaviour is in direct contrast with PETg as the polymer matrix (Fig. 4b), in which the addition of 10% additive always results in an increase in the maximum tensile strength. If the percentage of additive is increased further, a reduction in strength is observed in all cases with respect to the filament containing a 10% load, but never reaching values below those of the virgin PETg.

With regard to the additive that offers the highest strength to the parts, there is unanimity upon comparing the two polymeric bases, with metal powder emerging as the winner. Among the three additives, metal causes the least reduction in strength in the case of PLA as the base and achieves the greatest increase in strength with PETg.

Shell powder ranks in second place, followed by glass powder.

In the context of studying the tensile elastic modulus, it is noteworthy to observe that polymeric PLA matrix operates, when combined with the three additives, in higher values (Fig. 4c) than the observed when using PETg (Fig. 4d). Additionally, the trend for the first thermoplastic differs from that of the second. Specifically, when PLA is utilized as the matrix, the modulus values decrease below the virgin value upon incorporating 10% wt of any additive. Subsequently, these values increase beyond the previous value in all cases, except from seashells, that experiment a reduction of 33% respect the virgin one.

Conversely, when PETg is employed, the three additives demonstrate higher modulus values with a 10% wt of powder, as compared to the highest additive percentage.

In both cases, PLA and PETg, the additive exhibiting the highest modulus value is shells, while the lowest is glass.

3.2.2 Flexural properties

In the same way as with the tensile properties analysed in the previous subsection, the flexural properties are now studied for each type of additive and for each load percentage, respectively. The maximum bending strength and the elastic modulus of bending is regarded.

Once again, consistent with the results obtained from the tensile tests, the flexural strength of PLA (as illustrated in Fig. 5a) decreases with an increase in the percentage of the additive, irrespective of the type employed. It is interesting to note that with the maximum percentage incorporated, the metal hardly reduces its maximum flexural strength, while in the same way, with the addition of shell and glass powder, this reduction is significant, namely 38% and 42%, respectively.

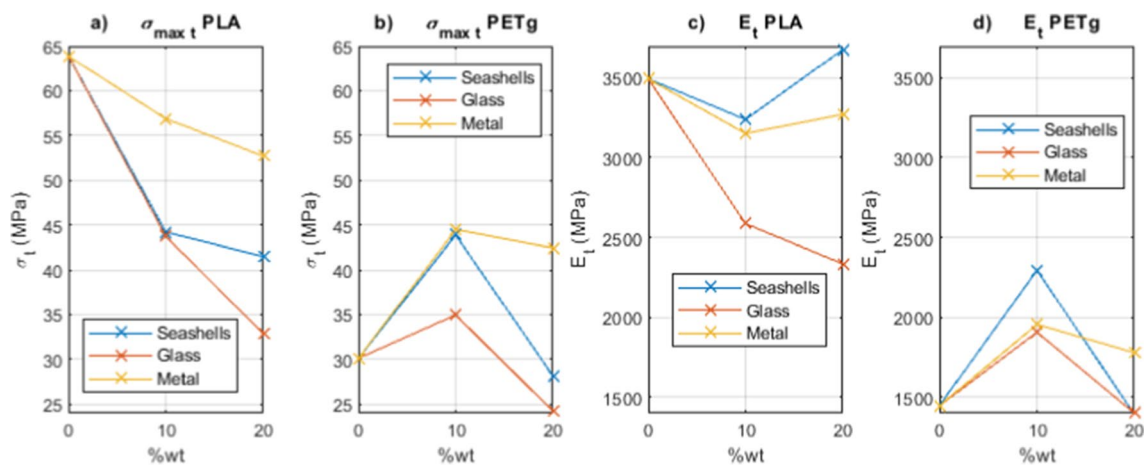


Fig. 4 Maximum tensile strength (a and b) and Young modulus (c and d) of PLA and PETg polymer matrix with different additive charges

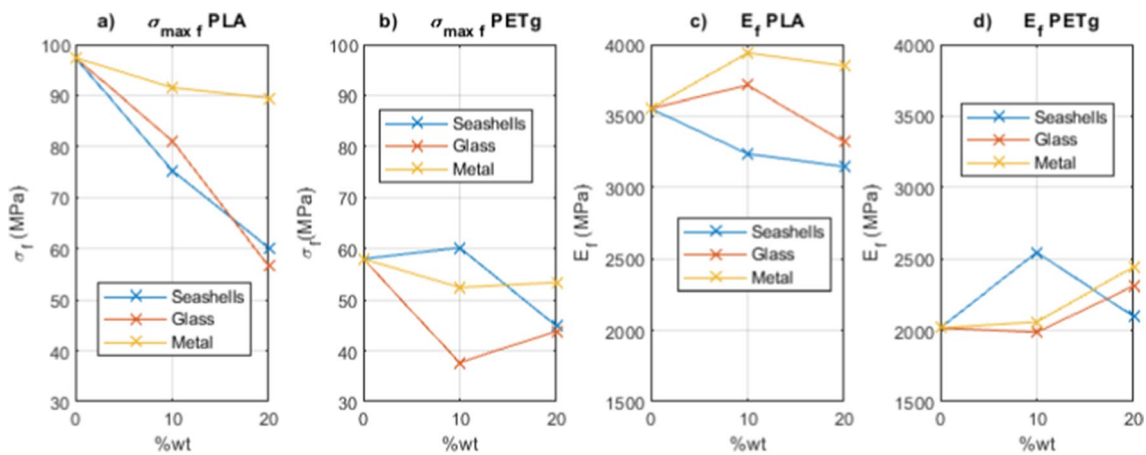


Fig. 5 Maximum flexural strength (a and b) and Young modulus (c and d) of PLA and PETg polymer matrix with different additive charges

Regarding PETg (Fig. 5b), the analysis reveals two distinct classifications of materials based on their behaviour: firstly, the filament containing shell powder additives and, secondly, those containing glass and metal additives, which exhibit similar trends. The latter demonstrates a greater reduction in strength with 10% wt added than with 20% wt. In the case of glass, parts subjected to lower weight percentage of additive exhibit 35% reduction in strength, whereas those under higher weight experience 24% reduction, both with respect to virgin PETg. Conversely, the addition of 10% wt of shell powder leads to 4% improvement in strength. However, by adding 20% wt of shell powder, the bending strength decreases by 23% when compared to the virgin material. When incorporating metal powder into the filament, the resistance is minimally reduced.

The results for the elastic flexural modulus of both PLA and PETg (Fig. 5c and d) exhibit a consistent trend with respect to the behaviour of the three additives. For PLA, the modulus increases for metal and glass with initial 10% wt loadings, but decreases as the additive content increases. In contrast, seashells decrease the modulus by 7% upon incorporation into the matrix, with a consistent value as the shell loading increases up to the maximum. For a PETg base, the modulus remains constant when 10% wt of glass or metal is incorporated. However, with 20% wt loading, the modulus increases by 25% for metal and 15% for glass. Incorporating 10% wt of shells increases the flexural modulus, but as the amount of additive increases, the modulus decreases and approaches the values of the virgin material.

3.3 Evaluation according to grain size and additive type

In this section, the influence on the mechanical properties of the use of powders of materials with different particle sizes is analysed, on the one hand, below 0.09 mm and on

the other hand below 0.18 mm. Both of them are assuming 20% of the weight of the filament.

3.3.1 Tensile properties

First, the influence of grain size on the ultimate tensile strength is analysed. As it can be seen in Fig. 6, for both PLA and PETg, the grain size of the metal does not affect tensile strength and modulus.

In PLA it is preferable to add 0.09 mm size powder in both shells and glass, as it exhibits greater results among the sizes analysed, both strength and modulus. In the case of PETg, the opposite behaviour can be observed in the strength with glass and seashells fillers.

In the case of the incorporation of metal fillers, the differences in terms of strength are not remarkable. It is true that a minimal increase in both strength and modulus is observed with a size of 0.18 mm rather than those with 0.09, in both polymeric matrices.

3.3.2 Flexural properties

In this case, the bending properties are evaluated with respect to the grain size used in the same way as in the previous section; the maximum bending strength and modulus are checked for the three loads for two different grain sizes: 0.09 and 0.18 mm.

In the case of bending properties in PLA (Fig. 7a), for all three loads, a smaller grain size is preferable, 12% higher maximum strength in metal, 34% in seashells and 31% with glass. While in terms of flexural modulus, it is ever more variation, 18% higher with metal powder, 49% with seashells and 30% with glass.

The behaviour of PETg additives differs from that of PLA. In terms of flexural strength (Fig. 7b), seashells exhibit the highest values, with a slight improvement even as grain

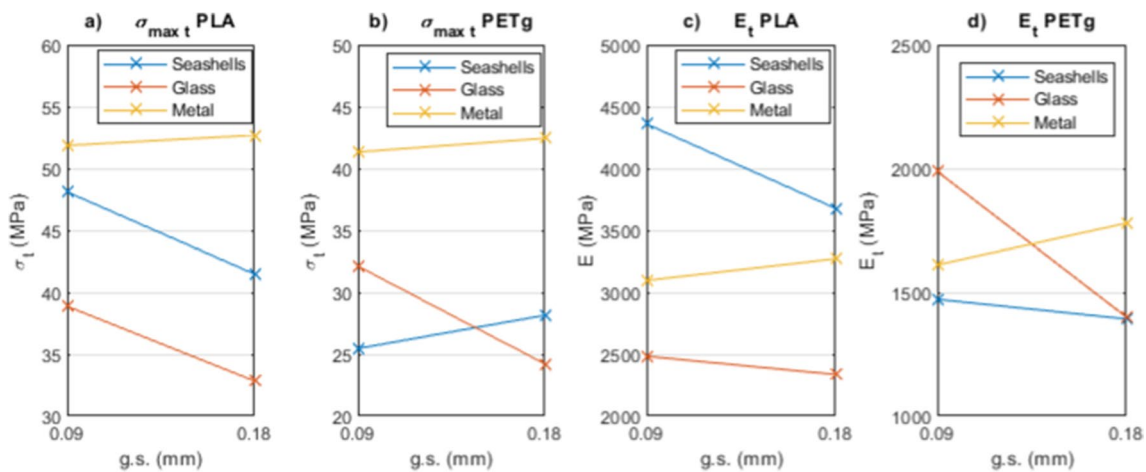


Fig. 6 Maximum tensile strength (a and b) and Young modulus (c and d) of PLA and PETg polymer matrix with different grain sizes of the powders

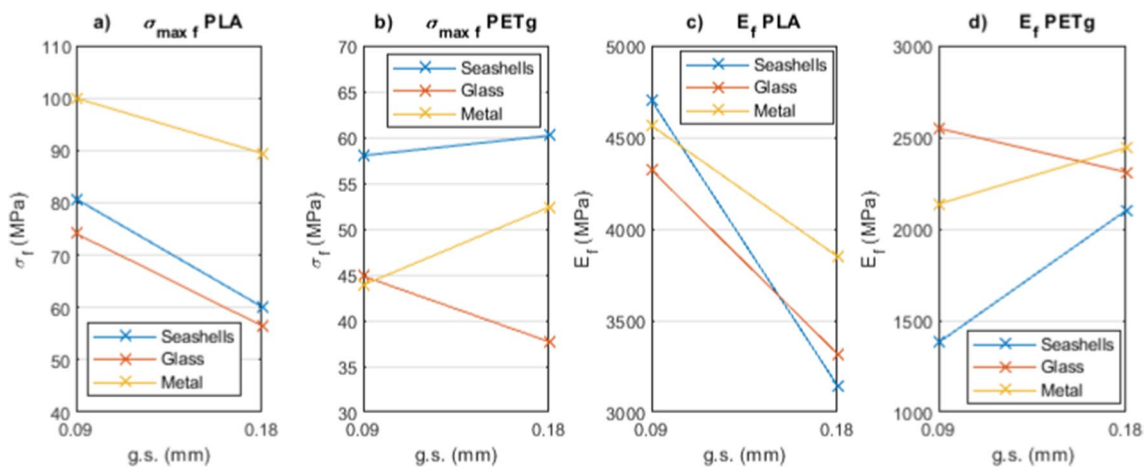


Fig. 7 Maximum flexural strength and Young modulus of PLA (left) and PETg (right) polymer matrix with different grain sizes of the powders

size increases. In the case of metal and glass, with a smaller grain size, they display similar strength; however, as the grain size increases, the strength of the metal increases while that of the glass decreases, both by 16%. The trend in elastic modulus (Fig. 7d) is similar for metal and seashells, with higher values observed in larger grain sizes, whereas in the case of glass, it results in the opposite trend.

3.4 Hardness evaluation

The results shown (Fig. 8) are an average of the previous measurements, which guarantee repeatability, as in no case is the deviation greater than 8%.

Initially, an evaluation is conducted to determine the hardness of the polymer matrices, namely PLA and PETG, when loaded with varying percentages (0%, 10% and 20%)

of shell powder, metal and glass, respectively. Figure 8 left illustrates the observed results, which demonstrate that the PLA specimens exhibit higher values of shore D hardness, with distinctive behaviour observed for each additive.

When PLA is employed as the polymer matrix, the hardness exhibits an increment of 9.5% upon the addition of 10% metal, whereas the same percentage results in negligible variation when shells or glass are utilized. These tendencies differ after the inclusion of 20% additive, as the metal content leads to a decrease of 15.21%, whereas both shells and glass exhibit an increase of 0.8% and 9%, respectively.

In contrast, PETG demonstrates hardness values that are 16% lower compared to PLA in its virgin state. Nevertheless, the behaviour of loaded PETG follows a consistent trend across all three cases. The addition of 10% seashells, glass, or metal results in a hardness average increase of 15.5%.

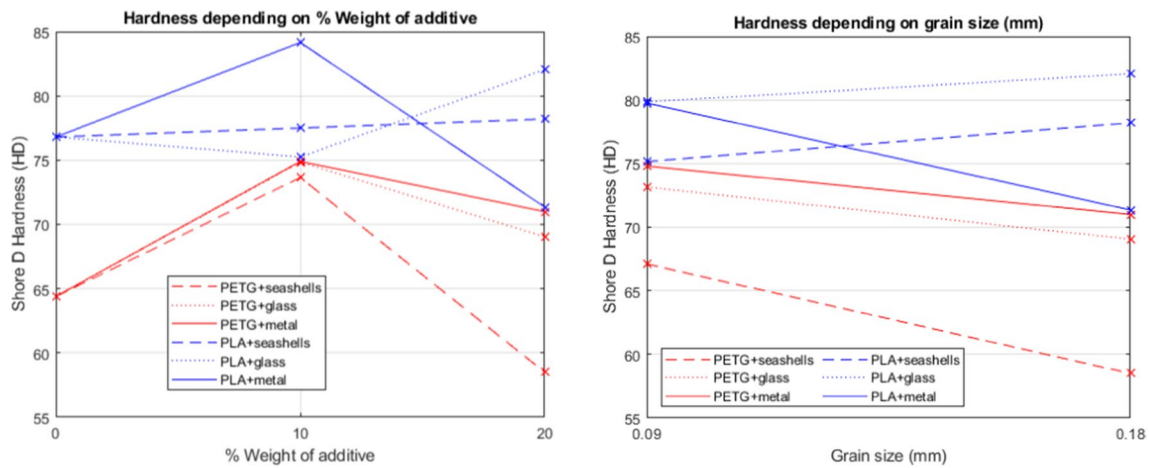


Fig. 8 Hardness depending on percentage of additive (left) and on grain size (right)

However, this value diminishes when additive in 20% are incorporated, displaying a more drastic decrease when seashells are used, while glass and metal experience lower reductions, of around 6%.

The present study includes a secondary evaluation, as depicted in Fig. 8 right, which focuses on comparing the hardness of six different material combinations based on the grain size of the utilized additive. The additives are categorized into two groups: those with fillers smaller than 0.18 mm and those with fillers smaller than 0.09 mm. Once again, distinct behaviours are observed depending on the polymeric matrices employed.

In the case of PLA, employing a larger grain size leads to an average increase in hardness of 2.2 HD points for glass, thereby exhibiting the highest HD hardness. Furthermore, an increase in grain size for shells results in a hardness increment of 3.05 HD points. Conversely, when using metal with a larger grain size, there is an average reduction of 8.4 HD points.

For PETg, all three additives exhibit a decrease in hardness when a larger grain size is employed.

Specifically, a decrease of 8.6 HD points is observed with shells, followed by reductions of 4.1 HD points with glass and 3.8 HD points with metal.

3.5 Microscopical analysis

Fractographies from the fracture surface, base layer, top layer and lateral are shown in Fig. 9 for PLA based samples and in Fig. 10 for PETg-based mixtures.

The external appearance of the samples containing the three different additives reveals good manufacturing results. One shared feature among them is the good sewing of the infill and the walls on the upper layer. However, darker areas on the base layer manifest higher level of gaps and,

therefore, worse sewing between parallel trajectories, specially on the mixture with seashell powder. This is due to the different viscosity of the three melted mixtures although the same printing temperature is used.

Through the different coloration of the seashell grains, which ranges from white to very dark brown, it is shown that this additive does not come only from one type of mollusc but is the result of the crushing of shells of different nature, such as clams and mussels.

It also can be seen that the shell powder adheres without creating hollows in the polymeric base, unlike what happens in metal, in which dark contours around the particles reveal the presence of air gaps that would affect the thermal properties.

From the lateral view, layer height seems to be slightly wavy, although this shape does not compromise their mechanical performance. This is mainly due to the fact that, in order to assure the absence of gaps between the walls and the infill, the skin overlap percentage was set to 50%.

All these comments about PLA with additives (Fig. 9) are also valid for those of PETG with the three types of powder (Fig. 10).

3.6 DSC/TGA

Mass loss and DSC were performed on the polymeric matrices' PLA and PETG (Fig. 11), previous to further analysis of thermal properties on mixtures polymer-powder.

The differences in terms of mass reduction are clear if both virgin plastics are compared. PLA begins its degradation first, at a temperature of approximately 303 °C, while PETG does so at 357 °C.

The first part of the curve of the DSC analysis corresponding to PLA reveals three relevant temperatures [51] in the creation and printing of filaments and prior to its

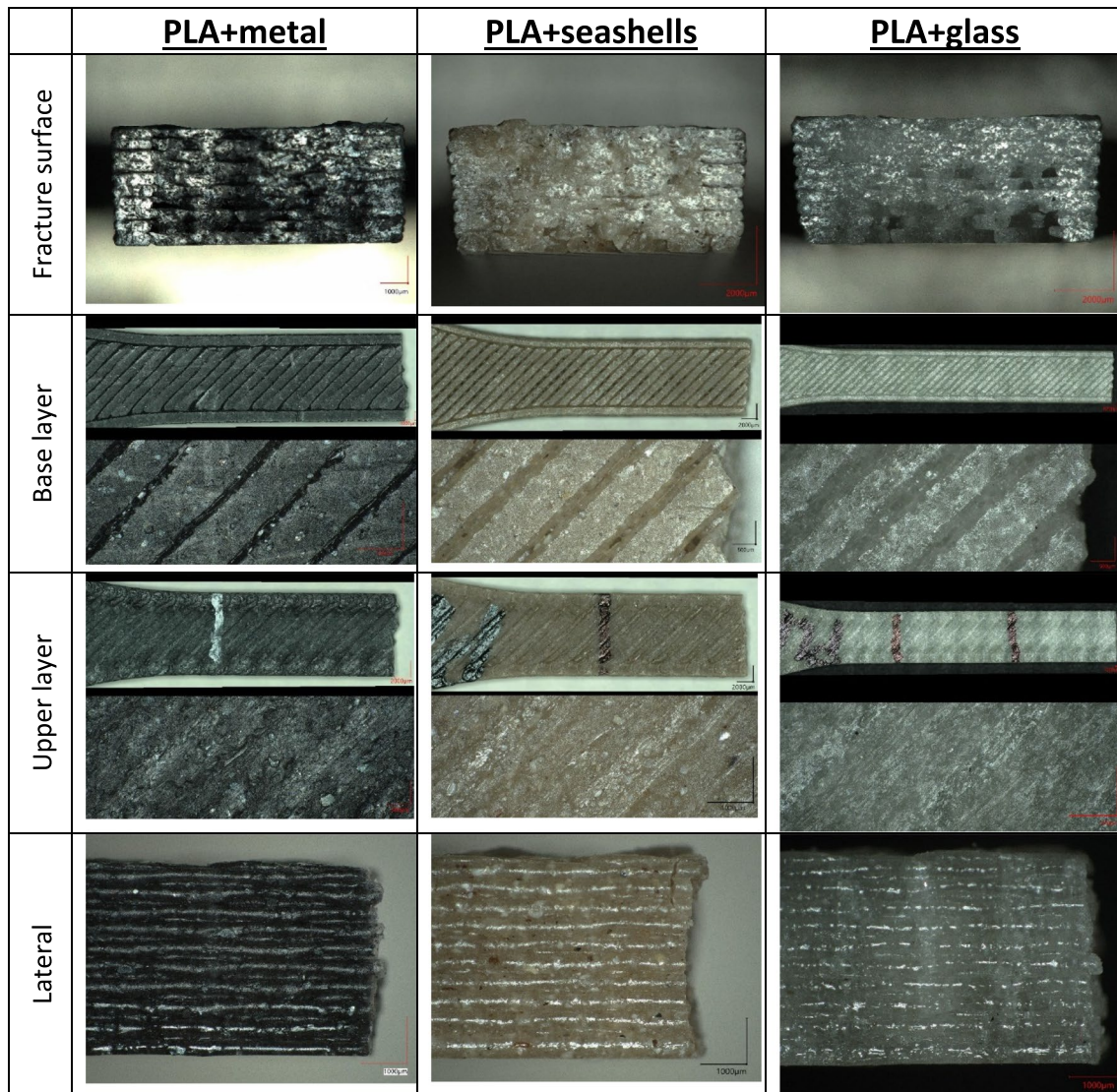


Fig. 9 Microscopical pictures of PLA based samples after the tensile test

degradation. The glass transition temperature T_v is the first to appear, revealing itself as a local minimum at $63\text{ }^\circ\text{C}$. Next, a maximum can be seen corresponding to the crystallization temperature T_c , which occurs at $113\text{ }^\circ\text{C}$. Thirdly, the melting temperature T_m is again represented by a local minimum at $148\text{ }^\circ\text{C}$. After this first zone, DSC stabilizes until the decomposition process begins and the mass falls. Here, the DSC shows that, to start this process, energy is absorbed until the production of the endothermic peak and at approximately $363\text{ }^\circ\text{C}$ due to release of gases prior to combustion of the material. Once the autoignition temperature is achieved, two consecutive peaks (393 and $500\text{ }^\circ\text{C}$) take place, corresponding to two different combustion phases [52, 53].

The difference in behaviour in the DSC of PETg compared to PLA is notable. Indications of T_v , T_c and T_m do

not reveal in the PETg due to the amorphous nature of this polymer [54], in contrast with the semi-crystalline structure of the PLA. When the degradation starts, that is, when mass starts to decay, two maxima are found in DSC analysis, of a magnitude six times greater than that of PLA, at temperatures of 430 and $527\text{ }^\circ\text{C}$. The first peak is associated with the thermal dissociation process where the decomposition of the polymer occurs, while the second peak, corresponding to the second step of mass loss, corresponds to the combustion of the mass of the residue that remains after the process of thermal dissociation [55, 56].

3.7 LFA evaluation

Diffusivity, specific heat and conductivity were obtained on PLA and PETg virgin, as well as with a

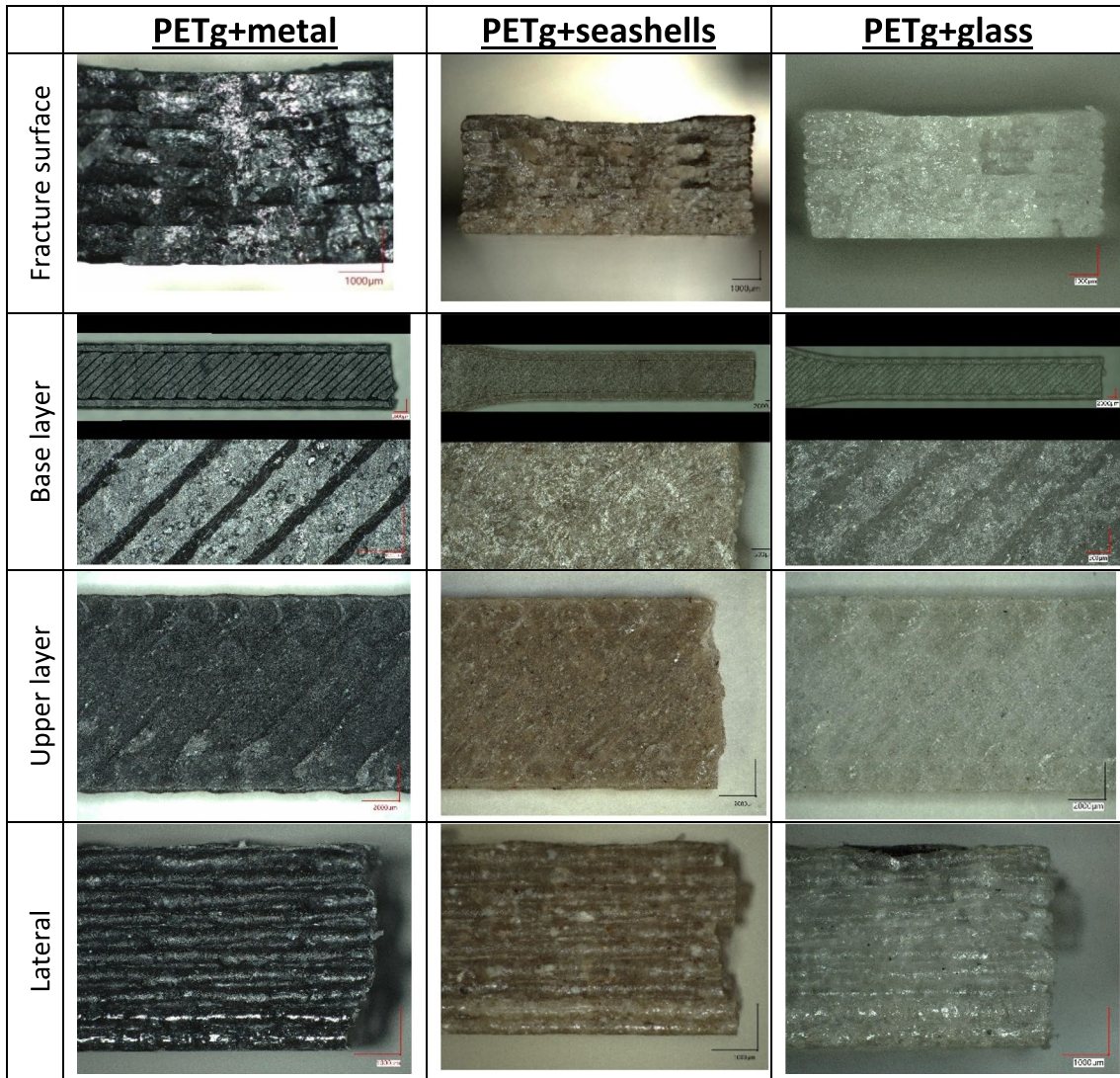


Fig. 10 Microscopical pictures of PETg based samples after the tensile test

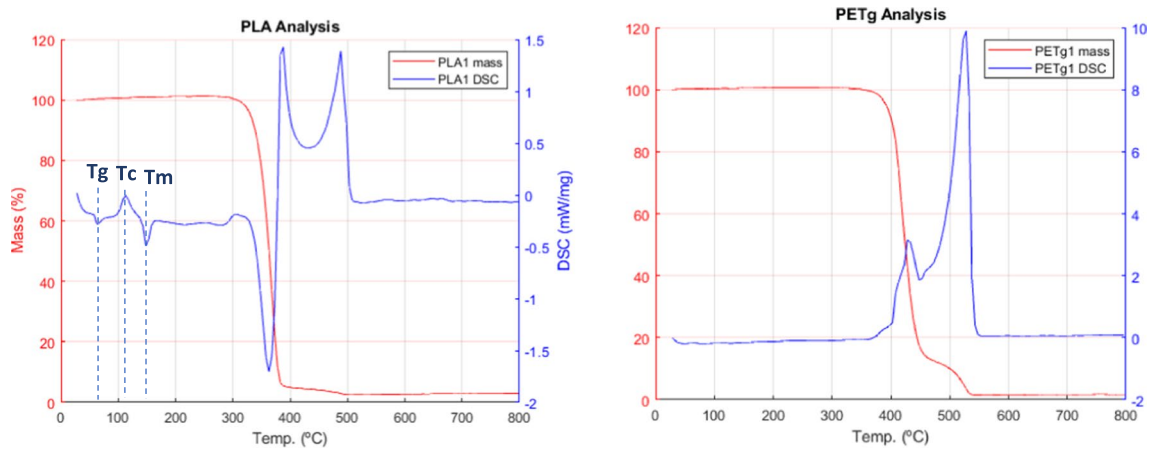


Fig. 11 DSC and TGA of virgin PLA and PETg

weight percentage of 20% of each of the three additives (seashells, glass and metal). Thus, eight different materials were considered on the LFA evaluation.

A considerable difference was found on the thermal diffusivity of PLA and PETg when including the powder additives (Fig. 12 left). Although the weight percentage added to both polymeric matrices (PLA and PETg) is the same, 20%, the effect provoked by them is different, with a completely different diffusivity ranking of the four materials evaluated. However, rankings of specific heat and conductivity are quite similar in mixtures with PLA and PETg (Fig. 12 centre and right), having both virgin polymers and polymers filled with glass the highest values in all the five temperatures analysed.

4 Discussion

Having presented the experimental findings, we now delve into a comprehensive discussion of the results obtained.

4.1 Mechanic results

The tensile and flexural strengths are reduced by increasing the percentage of additive, except in the case of PETg with a 10% weight of powder additive, in which there is an improvement to varying extents depending on the nature of the incorporated additive. The reduction of mechanical strength with the addition of a powder material is common, although some cases of improvement were also found in the literature, typically stemming from increased filament

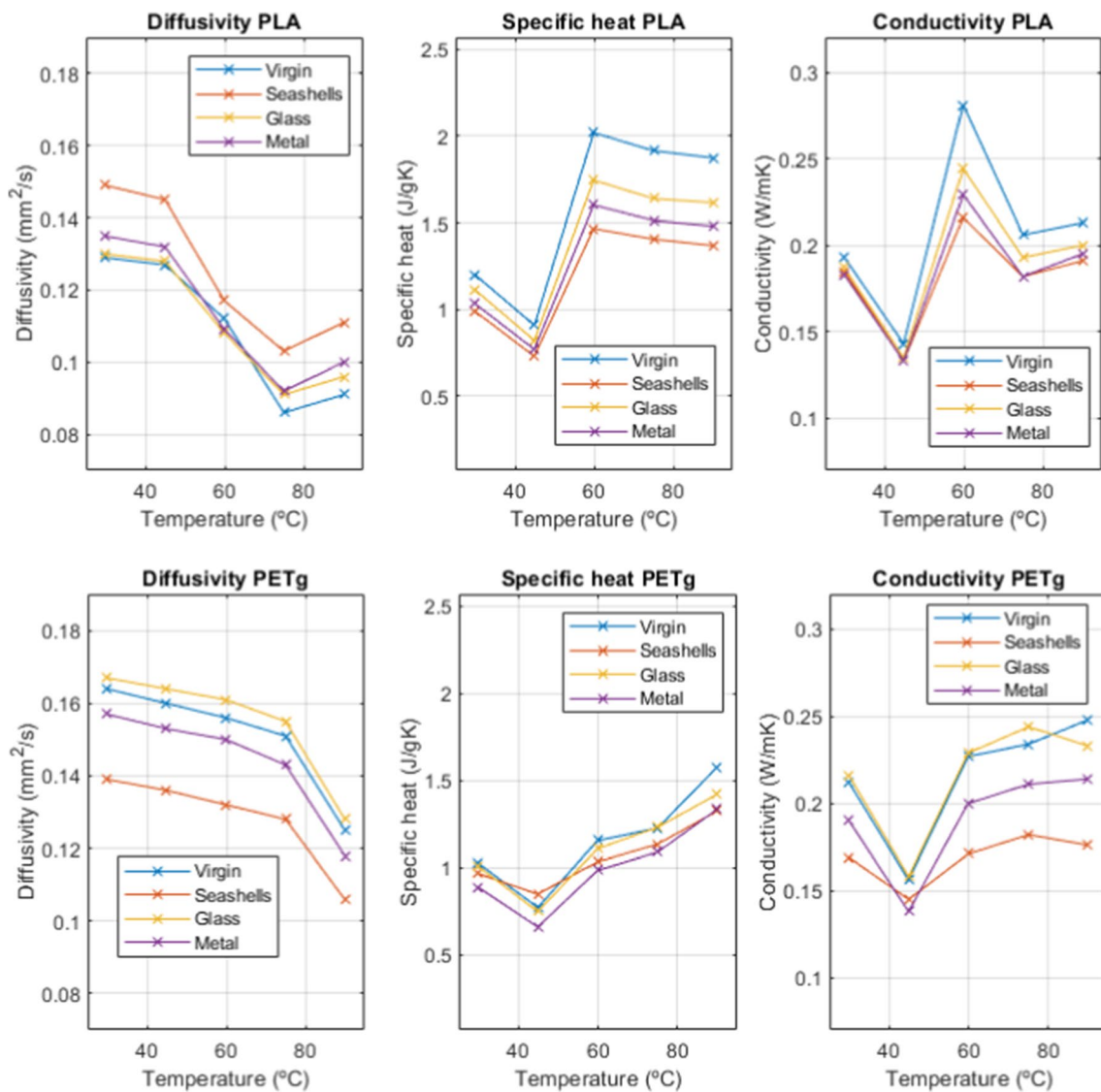


Fig. 12 Diffusivity, specific heat and conductivity of PLA (upper graphs) and PETg (lower graphs) with 20%wt powder additives

manufacturing complexity [11, 17, 22], more expensive equipment [18, 23, 57] and/or powder treatment [11, 22]. Because PLA is the most affordable and hence most commonly used plastic in FFF 3D printing, literature predominantly focuses on incorporating powder additives into this polymeric material, with hardly any literature regarding the inclusion of additives in PETG. Furthermore, the most widely studied additives include different types of metals (such as copper, nickel, aluminium, bromine, stainless steel)[5, 7, 18, 23, 46, 58–60], as well as calcium carbonate (CaCO_3) [11, 22, 57, 61–63], the material composing seashells. This information aids in making a comparative analysis between the results obtained in this paper and other studies. Figure 13 and Fig. 14 show the percentages of increase or decrease in resistance and elastic modulus relative to virgin PLA (without additives) depending on the weight percentage of additive for various material combinations found in the literature. It should be noted that this comparison is indicative since the printing parameters (nozzle size, speed, line width, pattern etc.) of the specimens are not similar, and these parameters significantly influence the mechanical properties of the printed part [3].

The red markers depicted in Fig. 13 and Fig. 14 represent the experimental results obtained in this study. Figure 13 illustrates a consistent trend wherein the addition of metal powder to a PLA matrix typically results in a reduction of the material's tensile strength by approximately 10 to 65%. Regarding the elastic modulus, although no clear pattern

emerges, deviations from virgin PLA generally remain within the range of $\pm 15\%$ across various cases. One can also observe that in most cases, the increase in the stiffness of the material evaluated compared to virgin PLA is accompanied by a reduction in its tensile strength, and vice versa. The findings concerning PLA augmented with metal, particularly sourced from mill scale in this investigation, closely align with prior research, showing no significant deviation. Notably, the decline in resistance is comparatively less pronounced than in some instances depicted in the graphical representations. Additionally, the flexural mechanical properties of PLA incorporating mill scale exhibit a favourable outlook, showcasing an enhancement in resistance and an increase in modulus when juxtaposed with other analysed cases where a decline in both parameters is apparent.

Regarding the combination of PLA with seashells or CaCO_3 (as shown in Fig. 14), most researchers incorporate minute quantities of powder additive, typically around 2.5%, with only a few cases exceeding 10%. Across all instances evaluated, flexural resistance consistently decreases by 20 to 52% compared to the resistance of pure PLA, with the experiments in this research falling within this range. However, the introduction of small amounts of powder additive tends to enhance tensile strength [11, 22, 57].

The manufacturing process of the material presented here is characterized by its simplicity, as both materials are mixed in a single extrusion step with a single-screw extruder to obtain the filament used for printing the samples. While

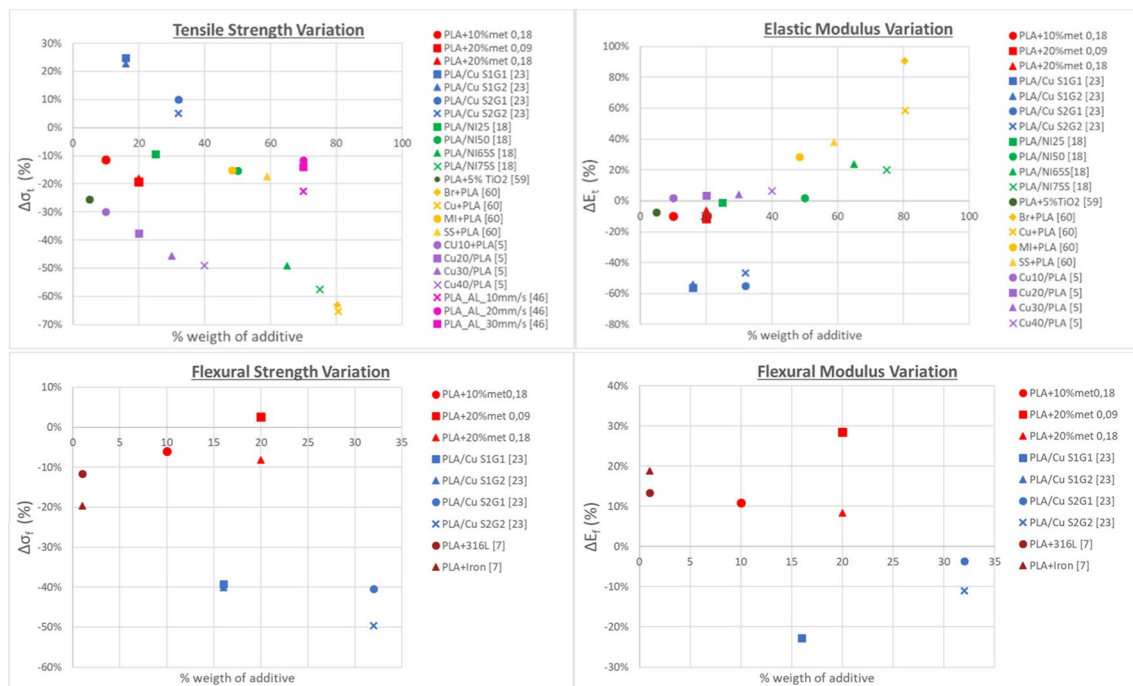


Fig. 13 Comparative evaluation of the improvement or deterioration of properties of mixtures PLA+metal found on the literature: **a** tensile strength, **b** tensile moduli, **c** flexural strength and **d** flexural moduli

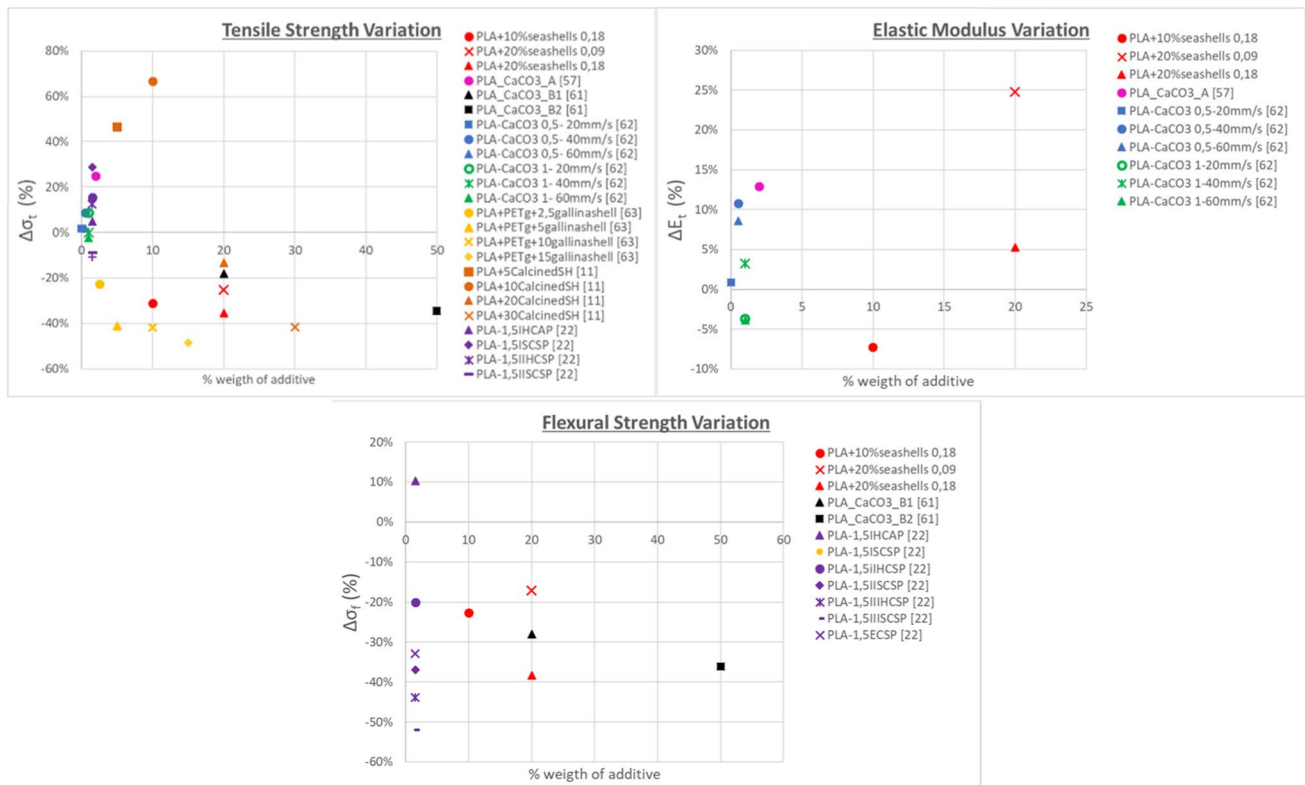


Fig. 14 Comparative evaluation of the improvement or deterioration of properties of mixtures PLA+CaCO₃ found on the literature: **a** tensile strength, **b** tensile moduli and **c** flexural strength

this may result in a weaker physical bond between polymer and additive (thus potentially increasing porosity) or an imperfectly homogeneous distribution of powder within the polymeric matrix, it does not lead to a drastic deterioration of mechanical properties compared to other authors who employ more complex procedures for filament production and samples manufacturing. Therefore, clear benefits are found in this uncomplicated material manufacturing method, the most important being the reduction of production costs and the decrease of plastic usage by employing industry by-products, which also have low or no cost, thereby promoting circular economy principles.

4.2 Thermal results

Regarding the analysis of the thermal conductivity of the mixtures created, some unexpected results stand out for which it is necessary to seek an explanation.

Despite the fact that, as an independent material, metal is more thermal conductive than polymers, glass or seashells, the addition of the metal to both polymer matrices does not cause an increment of the conductivity or specific heat above the other materials. Numerous reasons could explain this behaviour: volume of air gaps, size and quantity of the

powder grains, manufacturing process of the samples, quality of the filament and error range of the LFA machine.

To begin with, the incorporation of powder results in a higher number and volume of air gaps between the grains and the polymer, thereby diminishing the material’s heat transmission capacity. This clarifies why virgin PLA and PETg (with no powder at all) exhibit greater conductivity than all the analysed mixtures. Regarding the performance of additive polymers, it is largely influenced by the quantity and volume of grains within the matrix. The granulometry of the various powder additions provides insight into the grain size. The three powders utilized in the thermal samples have a size below 0.09 mm. However, the size distribution between 0 and 0.09 mm varies, with metal having a higher percentage of finer powder (10.6% lower than 0.02 mm), seashells containing more of the coarser powder (0% lower than 0.02 mm) and glass falling between the two with 4.7%. Moreover, it is important to note that the amount of powder included in the polymer matrix is measured as a percentage of weight, not volume. Consequently, for the same volume of sample, the lower the density of the additive, the greater the volume of powder in the mixture. Accordingly, samples with seashells contain a higher volume of powder (22% v), followed by glass (20% v), and lastly, metal (9.8% v). The presence of air gaps or

pores at the grain-polymer interface is also influenced by the external surface and shape of the grains [64]. Additionally, the manufacturing process of the samples, along with the disparity in printing temperature between PLA and PETg samples, can lead to variations in the viscosity of the melted material extruded from the nozzle, consequently affecting the shapes and dimensions of these gaps, and thus their conductivity. Finally, the quality of the extruded filament plays a critical role and has a more significant impact on the thermal properties than on the mechanical ones. The combination of all these factors explained before could influence on each mixture sample in different proportions, leading to the results of Fig. 12, that do not follow a consistent ranking in PLA and in PETg when adding the three different powders.

Among all the results pertaining to conductivity, diffusivity and specific heat, one material notably distinguishes itself from the others due to its comparatively lower outcomes and its divergent temperature trend at 45°C. This material is PETg with 20% w addition of seashells. Upon scrutinizing the densities of all LFA samples (Table 5), it becomes evident that an anomalous outcome is observed, whereby the incorporation of powder fails to augment its density in comparison to the virgin material, as observed in the remaining cases. Once again, this discrepancy may stem from the higher proportion of voids generated between the polymer and material or from a chemical reaction between them leading to a reduction in the mass of either component. This alteration, whether physical or chemical in nature, diminishes the heat transmission capability of this blend.

There is limited literature available regarding thermal conductivity values in 3D printed samples with additives of different natures, as well as the temperature-dependent conductivity variances. However, the research findings generally indicate an enhancement in thermal properties (specifically conductivity) upon the inclusion of metallic particles such as copper [5] and various metallic oxides (zinc [65], cobalt, iron and nickel [66]) even combined with carbon nanotubes in some cases, exhibiting a conductivity up to four times higher compared to the base material. This observed

behaviour contrasts sharply with the outcomes of this study, where the addition of powder from different materials results in a deterioration of conductivity. Consequently, despite achieving an improvement in tensile mechanical properties with a 10%w powder additive, if enhanced thermal conductivity is desired, alternative filament manufacturing techniques need to be explored to mitigate the occurrence and magnitude of created pores.

With regard to the temperature-dependent variation observed in the experiment, Feng et al. [11] reported a progressive reduction in conductivity values with increasing temperature ranging from 50 to 120°C, both in samples composed of 100% PLA and in mixtures of PLA, PETg and g-C₃N₄ in various proportions, which represents a significant disparity compared to the findings of this paper. Although the present study does not include samples combining PLA and PETg, markedly different outcomes are obtained for each of the two materials studied independently, albeit with a common observation of a conductivity minimum at a temperature of 45°C. Subsequent to this minimum, the conductivity of PETg improves with temperature, whereas PLA exhibits a rapid increase leading to a peak at 60°C, followed by a decline. Due to the dearth of substantial literature on this matter, the underlying causes of these behaviours and the reasons for these disparities remain unclear, thus necessitating a more detailed investigation of this phenomenon, complemented by chemical and microscopic analyses, to shed further light on the subject.

5 Conclusions

This study has provided a comprehensive analysis of the mechanical and thermal properties of PLA and PETg polymeric matrices reinforced with varying proportions of three powders: seashells, metal and glass. The results indicate that:

- Adding 10%w powder of any of the three varieties to PETg increases tensile strength of the material up to 48%, best with metal powder (mill scale), even at 20%w, showing a 41% increase.
- Conversely, adding powder to PLA worsens mechanical properties, a common phenomenon that has been evidenced in the literature review on the discussion section. However, this deterioration is not accompanied by a stiffening of the material; instead, the elastic modulus is also decreased.
- Metal grain size has minimal impact. A grain size lower than 0.09 mm is optimal for PLA.
- Contrary to expectations, thermal conductivity measured in polymers blended with powder additives is lower than that of the virgin polymers. Among the various hypotheses considered, the formation of air voids between the

Table 5 Density of the LFA samples

Material	Density (g/cm ³)
PLA	1.245
PLA+20%w metal	1.313
PLA+20%w seashells	1.258
PLA+20%w glass	1.296
PETg	1.263
PETg+20%w metal	1.362
PETg+20%w seashells	1.254
PETg+20%w glass	1.284

powder and the polymer matrix appears to be the most likely explanation, supported by density results and visual and microscopic evaluations.

- PLA and PETg mixtures show different thermal property evolutions, notably at 60–75°C, due to PLA's transition temperature around 63°C.

Future investigations will concentrate on conducting a more in-depth analysis of thermal behaviour. DSC tests will be conducted on all mixtures to augment the study. The uncertainties surrounding the results, attributed to the dispersion and adhesion of powder additives on the polymer, will be evaluated using a scanning electron microscope. The assessment of the environmental impact of the mixtures will also be the subject of future investigation, involving the conduct of a life cycle analysis.

The feasibility of using industrial process powder to produce 3D printing filaments with optimistic mechanical properties has been demonstrated. However, if enhanced thermal properties are needed, alternative approaches must be explored while maintaining focus on manufacturing simplicity and promoting circular economy principles. Future efforts will aim to improve results by exploring different industry by-products for better compatibility with the polymeric matrix. Simplifying the manufacturing process may involve considering chemical additives to address air space formation. Another option is producing additive-enhanced filament from powdered polymeric material, depending on supplier availability to avoid complexity and increased costs.

Acknowledgements The authors want to thank the following entities for their contribution: LAGUC laboratory, for providing the equipment to carry out the mechanical tests; GIDAI, for carrying out the thermal tests; and FCC Ámbito, Celsa Group and Abonomar, for supplying the additives.

Funding Open Access funding provided thanks to the CRUE-CSIC agreement with Springer Nature. This work has been co-financed by the Spanish Ministry of Science and Innovation through the R+D+i projects 2020 call, under the project “Fostering the circular economy and low CO₂ technologies through the additive manufacturing (3DCircle)” (PID2020-112851RA-I00).

Declarations

Competing interests The authors declare no competing interests.

Disclaimer This work reflects the authors' opinion, so the authorities of the programme are not responsible for the use of the information here included.

Open Access This article is licensed under a Creative Commons Attribution 4.0 International License, which permits use, sharing, adaptation, distribution and reproduction in any medium or format, as long as you give appropriate credit to the original author(s) and the source, provide a link to the Creative Commons licence, and indicate if changes were made. The images or other third party material in this article are included in the article's Creative Commons licence, unless indicated

otherwise in a credit line to the material. If material is not included in the article's Creative Commons licence and your intended use is not permitted by statutory regulation or exceeds the permitted use, you will need to obtain permission directly from the copyright holder. To view a copy of this licence, visit <http://creativecommons.org/licenses/by/4.0/>.

References

1. Mohanavel V, Ashraff Ali KS, Ranganathan K et al (2021) The roles and applications of additive manufacturing in the aerospace and automobile sector. *Mater Today Proc* 47:405–409. <https://doi.org/10.1016/j.matpr.2021.04.596>
2. Dunham S, Mosadegh B, Romito EA, Zgaren M (2018) Applications of 3D printing. In: *3D Printing Applications in Cardiovascular Medicine*. Elsevier, pp 61–78
3. Castanon-Jano L, Palomera-Obregon P, Blanco-Fernandez E, Indacoechea-Vega I (2023) Analysis of manufacturing and material parameters in 3D-printed polylactic acid (PLA) parts filled with glass powder: mechanical, economic, and environmental assessment. *Int J Adv Manuf Technol*. <https://doi.org/10.1007/s00170-023-12023-7>
4. Darsin M, Sabariman WA, Trifiananto M, Fachri BA (2023) Flexural properties of metal 3D printing products using PLA-stainless steel filament. *AIP Conference Proceedings*
5. Vu MC, Jeong T-H, Kim J-B et al (2021) 3D printing of copper particles and poly(methyl methacrylate) beads containing poly(lactic acid) composites for enhancing thermomechanical properties. *J Appl Polym Sci* 138:49776. <https://doi.org/10.1002/app.49776>
6. Lee J, Lee H, Cheon K-H et al (2019) Fabrication of poly(lactic acid)/Ti composite scaffolds with enhanced mechanical properties and biocompatibility via fused filament fabrication (FFF)-based 3D printing. *Addit Manuf* 30:100883. <https://doi.org/10.1016/j.addma.2019.100883>
7. Jiang D, Ning F, Wang Y (2021) Additive manufacturing of biodegradable iron-based particle reinforced polylactic acid composite scaffolds for tissue engineering. *J Mater Process Technol* 289:116952. <https://doi.org/10.1016/j.jmatprotec.2020.116952>
8. Tao Y, Wang H, Li Z et al (2017) Development and application of wood flour-filled polylactic acid composite filament for 3d printing. *Materials* 10:339. <https://doi.org/10.3390/ma10040339>
9. Aumnate C, Soatthyanon N, Makmoon T, Potiyaraj P (2021) Polylactic acid/kenaf cellulose biocomposite filaments for melt extrusion based-3D printing. *Cellulose* 28:8509–8525. <https://doi.org/10.1007/s10570-021-04069-1>
10. Figueroa-Velarde V, Diaz-Vidal T, Cisneros-López EO et al (2021) Mechanical and physicochemical properties of 3d-printed agave fibers/poly(Lactic acid) biocomposites. *Materials* 14:3111. <https://doi.org/10.3390/ma14113111>
11. Razali MS, Khimeche K, Melouki R et al (2022) Preparation and properties enhancement of poly(lactic acid)/calcined-seashell biocomposites for 3D printing applications. *J Appl Polym Sci* 139:51591. <https://doi.org/10.1002/app.51591>
12. Ankor MJ, Tyler JJ, Hughes CE (2019) Development of an autonomous, monthly and daily, rainfall sampler for isotope research. *J Hydrol (Amst)* 575:31–41. <https://doi.org/10.1016/j.jhydrol.2019.04.074>
13. Devra RS, Srivastava N, Vadali M, Arora A (2022) Polymer filament extrusion using LDPE waste polymer: effect of processing temperature. *Proceedings of ASME 2022 17th International Manufacturing Science and Engineering Conference, MSEC 2022 1*. <https://doi.org/10.1115/MSEC2022-85586>
14. Lanzotti A, Martorelli M, Maietta S et al (2019) A comparison between mechanical properties of specimens 3D printed with

- virgin and recycled PLA. *Procedia CIRP* 79:143–146. <https://doi.org/10.1016/J.PROCIR.2019.02.030>
15. Cruz Sanchez FA, Boudaoud H, Hoppe S, Camargo M (2017) Polymer recycling in an open-source additive manufacturing context: mechanical issues. *Addit Manuf* 17:87–105. <https://doi.org/10.1016/J.ADDMA.2017.05.013>
 16. Wang L, Cao QL, Cao Y (2013) Study on the properties of coffee carbon filament yarns. *Adv Mater Res* 821:64–67. <https://doi.org/10.4028/www.scientific.net/AMR.821-822.64>
 17. Díaz-García Á, Law JY, Felix M et al (2022) Functional, thermal and rheological properties of polymer-based magnetic composite filaments for additive manufacturing. *Mater Des* 219:110806. <https://doi.org/10.1016/j.matdes.2022.110806>
 18. Karimi N, Fayazfar H (2023) Development of highly filled nickel-polymer feedstock from recycled and biodegradable resources for low-cost material extrusion additive manufacturing of metals. *J Manuf Process* 107:506–514. <https://doi.org/10.1016/j.jmapro.2023.10.064>
 19. Rasouli A, Azdast T, Mohammadzadeh H et al (2022) Morphological properties and mechanical performance of polylactic acid scaffolds fabricated by a novel fused filament fabrication/gas foaming coupled method. *Int J Adv Manuf Technol* 119:7463–7474. <https://doi.org/10.1007/s00170-022-08743-x>
 20. Azdast T, Hasanzadeh R (2021) Polylactide scaffold fabrication using a novel combination technique of fused deposition modeling and batch foaming: dimensional accuracy and structural properties. *Int J Adv Manuf Technol* 114:1309–1321. <https://doi.org/10.1007/s00170-021-06915-9>
 21. Raghavendran HRB, Natarajan E, Mohan S et al (2021) The functionalization of the electrospun PLLA fibrous scaffolds reduces the hydrogen peroxide induced cytokines secretion in vitro. *Mater Today Commun* 26:101812. <https://doi.org/10.1016/j.mtcomm.2020.101812>
 22. Yang F, Ye X, Zhong J et al (2023) Recycling of waste crab shells into reinforced poly (lactic acid) biocomposites for 3D printing. *Int J Biol Macromol* 234:122974. <https://doi.org/10.1016/j.jbiomac.2022.12.193>
 23. Simon Ž, Stojcevski F, Dharmasiri B et al (2024) Circular economy-driven additive manufacturing: a model for recycling PLA/copper composites through multi-extrusion processing. *J Ind Eng Chem* 130:392–400. <https://doi.org/10.1016/j.jiec.2023.09.044>
 24. Mihankhah P, Azdast T, Mohammadzadeh H et al (2023) Fused filament fabrication of biodegradable polylactic acid reinforced by nanoclay as a potential biomedical material. *J Thermoplast Compos Mater* 36:961–983. <https://doi.org/10.1177/08927057211044185>
 25. Natarajan E, Sekar T, Markandan K et al (2024) Structural integrity and mechanical behaviour of magnesium oxide (MgO) as reinforcement in PLA-HDPE composite. *Emerg Mater*:1–12. <https://doi.org/10.1007/s42247-024-00650-z>
 26. Cao D (2024) Increasing strength and ductility of extruded polylactic acid matrix composites using short polyester and continuous carbon fibers. *Int J Adv Manuf Technol* 130:3631–3647. <https://doi.org/10.1007/s00170-023-12887-9>
 27. Cao D, Bouzolin D, Lu H, Griffith DT (2023) Bending and shear improvements in 3D-printed core sandwich composites through modification of resin uptake in the skin/core interphase region. *Compos Part B Eng* 264:110912. <https://doi.org/10.1016/j.compositesb.2023.110912>
 28. Cao D (2023) Investigation into surface-coated continuous flax fiber-reinforced natural sandwich composites via vacuum-assisted material extrusion. *Prog Addit Manuf*:1–15. <https://doi.org/10.1007/s40964-023-00508-6>
 29. Cicero S, Martínez-Mata V, Castanon-Jano L et al (2021) Analysis of notch effect in the fracture behaviour of additively manufactured PLA and graphene reinforced PLA. *Theor Appl Fract Mech* 114:103032. <https://doi.org/10.1016/j.tafmec.2021.103032>
 30. Villada JT, Lyngdoh GA, Paswan R et al (2023) Evaluating the adhesion response of acrylonitrile-butadiene-styrene (ABS)/thermoplastic polyurethane (TPU) fused interface using multiscale simulation and experiments. *Mater Des* 232:112155. <https://doi.org/10.1016/j.matdes.2023.112155>
 31. Cicero S, Martínez-Mata V, Alonso-Estebanez A et al (2020) Analysis of notch effect in 3D-printed ABS fracture specimens Containing U-Notches. *Materials* 13:4716. <https://doi.org/10.3390/ma13214716>
 32. Clarke T, Hosseini A (2023) Effects of print parameters on tensile characteristics of additively manufactured polyethylene terephthalate-glycol (PETG). *Int J Adv Manuf Technol* 125:4953–4974. <https://doi.org/10.1007/s00170-023-11003-1>
 33. Steck P, Scherb D, Witzgall C et al (2023) Design and additive manufacturing of a passive ankle-foot orthosis incorporating material characterization for fiber-reinforced PETG-CF15. *Materials* 16:3503. <https://doi.org/10.3390/ma16093503>
 34. Ermolai V, Sober A, Lang A (2023) Characterisation of the shape memory effect of PET polymer by FFF 3D printing. *ESAFORM* 2023. pp 93–100. <https://doi.org/10.21741/9781644902479-11>
 35. Bin PJ, An SH, Jung JW, Lee JU (2023) Three-dimensional printing of recycled polypropylene and activated carbon coatings for harmful gas adsorption and antibacterial properties. *Polymers (Basel)* 15:1173. <https://doi.org/10.3390/polym15051173>
 36. Bruère VM, Lion A, Holtmannspötter J, Jöhrlitz M (2023) The influence of printing parameters on the mechanical properties of 3D printed TPU-based elastomers. *Prog Addit Manuf* 8:693–701. <https://doi.org/10.1007/s40964-023-00418-7>
 37. Vaucher J, Demongeot A, Michaud V, Leterrier Y (2022) Recycling of bottle grade PET: influence of HDPE contamination on the microstructure and mechanical performance of 3D printed parts. *Polymers (Basel)* 14:5507. <https://doi.org/10.3390/polym14245507>
 38. Zhang J, Chen D-R, Chen S-C (2022) A review of emission characteristics and control strategies for particles emitted from 3D fused deposition modeling (FDM) printing. *Build Environ* 221:109348. <https://doi.org/10.1016/j.buildenv.2022.109348>
 39. Sandanamsamy L, Harun WSW, Ishak I et al (2023) A comprehensive review on fused deposition modelling of polylactic acid. *Prog Addit Manuf* 8:775–799. <https://doi.org/10.1007/s40964-022-00356-w>
 40. Gomes Correia VM, Pereira N, Perinka N et al (2022) Printed 3D gesture recognition thermoformed half sphere compatible with in-mold electronic applications. *Adv Eng Mater* 24:2200730. <https://doi.org/10.1002/adem.202200730>
 41. Sivakumar NK, Palaniyappan S, Vishal K et al (2023) Crushing behavior optimization of octagonal lattice-structured thin-walled 3D printed carbon fiber reinforced PETG (CF/PETG) composite tubes under axial loading. *Polym Compos* 45(2):1228–1249. <https://doi.org/10.1002/pc.27848>
 42. Kumar R, Sharma H, Saran C et al (2022) A comparative study on the life cycle assessment of a 3D printed product with PLA, ABS & PETG Materials. *Procedia CIRP* 107:15–20. <https://doi.org/10.1016/j.procir.2022.04.003>
 43. Ulkir O (2023) Energy-consumption-based life cycle assessment of additive-manufactured product with different types of materials. *Polymers (Basel)* 15:1466. <https://doi.org/10.3390/polym15061466>
 44. Ly O, Yoris-Nobile AI, Sebaibi N et al (2021) Optimisation of 3D printed concrete for artificial reefs: biofouling and mechanical analysis. *Constr Build Mater* 272:121649. <https://doi.org/10.1016/J.CONBUILDMAT.2020.121649>

45. Boukhelf F, Sebaibi N, Boutouil M et al (2022) On the properties evolution of eco-material dedicated to manufacturing artificial reef via 3D printing: long-term interactions of cementitious materials in the marine environment. *Sustainability* 14:9353. <https://doi.org/10.3390/SU14159353>
46. Hasanzadeh R, Mihankhah P, Azdast T et al (2023) Optimization of process parameters of fused filament fabrication of polylactic acid composites reinforced by aluminum using Taguchi approach. *Metals* (Basel) 13:1013. <https://doi.org/10.3390/met13061013>
47. Hasanzadeh R, Mihankhah P, Azdast T et al (2024) Process-property relationship in polylactic acid composites reinforced by iron microparticles and $3D$ printed by fused filament fabrication. *Polym Eng Sci* 64:399–411. <https://doi.org/10.1002/pen.26556>
48. UNE-EN ISO 527-1:2020 Plásticos. Determinación de las propiedades en tracción. Parte 1: Principios generales. Accessed 2 Nov 2022
49. UNE-EN ISO 178:2020 Plásticos. Determinación de las propiedades de flexión. Accessed 2 Nov 2022
50. Parker WJ, Jenkins RJ, Butler CP, Abbott GL (1961) Flash method of determining thermal diffusivity, heat capacity, and thermal conductivity. *J Appl Phys* 32:1679–1684. <https://doi.org/10.1063/1.1728417>
51. Ali F, Kalva SN, Mroue KH et al (2023) Degradation assessment of Mg-Incorporated 3D printed PLA scaffolds for biomedical applications. *Bioprinting* 35:e00302. <https://doi.org/10.1016/j.bprint.2023.e00302>
52. Xiang S, Feng L, Bian X et al (2020) Evaluation of PLA content in PLA/PBAT blends using TGA. *Polym Test* 81:106211. <https://doi.org/10.1016/j.polymertesting.2019.106211>
53. Reich G (1997) Use of DSC to study the degradation behavior of PLA and PLGA microparticles. *Drug Dev Ind Pharm* 23:1177–1189. <https://doi.org/10.3109/03639049709146155>
54. Latko-Durałek P, Dydek K, Boczkowska A (2019) Thermal, rheological and mechanical properties of PETG/rPETG blends. *J Polym Environ* 27:2600–2606. <https://doi.org/10.1007/s10924-019-01544-6>
55. Fabia J, Gawłowski A, Rom M et al (2020) PET Fibers Modified with Cloisite Nanoclay. *Polymers* (Basel) 12:774. <https://doi.org/10.3390/polym12040774>
56. Dong X, Chen L, Duan R-T, Wang Y-Z (2016) Phenylmaleimide-containing PET-based copolyester: cross-linking from $2\pi + \pi$ cycloaddition toward flame retardance and anti-dripping. *Polym Chem* 7:2698–2708. <https://doi.org/10.1039/C6PY00183A>
57. Zarei M, Hosseini Nikoo MM, Alizadeh R, Askarinya A (2024) Synergistic effect of CaCO₃ addition and in-process cold atmospheric plasma treatment on the surface evolution, mechanical properties, and in-vitro degradation behavior of FDM-printed PLA scaffolds. *J Mech Behav Biomed Mater* 149:106239. <https://doi.org/10.1016/j.jmbbm.2023.106239>
58. Petousis M, Vidakis N, Mountakis N et al (2022) Multifunctional material extrusion 3D-printed antibacterial polylactic acid (PLA) with binary inclusions: the effect of cuprous oxide and cellulose nanofibers. *Fibers* 10:52. <https://doi.org/10.3390/fib10060052>
59. Pemas S, Xanthopoulou E, Terzopoulou Z et al (2023) Exploration of methodologies for developing antimicrobial fused filament fabrication parts. *Materials* 16:6937. <https://doi.org/10.3390/ma16216937>
60. Vakharia VS, Kuentz L, Salem A et al (2021) Additive manufacturing and characterization of metal particulate reinforced polylactic acid (PLA) polymer composites. *Polymers* (Basel) 13:3545. <https://doi.org/10.3390/polym13203545>
61. Varga P, Lorinczy D, Toth L et al (2019) Novel PLA-CaCO₃ composites in additive manufacturing of upper limb casts and orthotics—a feasibility study. *Mater Res Express* 6:045317. <https://doi.org/10.1088/2053-1591/aafdbc>
62. Seyedzavvar M, Boğa C, Zehir B (2023) Experimental study and hybrid optimization of material extrusion process parameters for enhancement of fracture resistance of biodegradable nanocomposites. *Eng Fail Anal* 150:107294. <https://doi.org/10.1016/j.engfailanal.2023.107294>
63. Selçuk Pekdemir S, Onay H, Özen Öner E et al (2024) Valorization of bio-calcium carbonate based *Chamelea gallina* shell waste fillers in shape memory polymer composites. *J Appl Polym Sci* 141:e55187. <https://doi.org/10.1002/app.55187>
64. Islam S, Bhat G, Sikdar P (2023) Thermal and acoustic performance evaluation of 3D-printable PLA materials. *J Build Eng* 67:105979. <https://doi.org/10.1016/j.jobbe.2023.105979>
65. Tan MA, Yeoh CK, Teh PL et al (2023) Effect of zinc oxide suspension on the overall filler content of the PLA/ZnO composites and cPLA/ZnO composites. *e-Polymers* 23:20228113. <https://doi.org/10.1515/epoly-2022-8113>
66. Homa P, Wenelska K, Mijowska E (2020) Enhanced thermal properties of poly(lactic acid)/MoS₂/carbon nanotubes composites. *Sci Rep* 10:740. <https://doi.org/10.1038/s41598-020-57708-1>

Publisher's note Springer Nature remains neutral with regard to jurisdictional claims in published maps and institutional affiliations.